Published by Avanti Publishers

Journal of Advanced Thermal Science Research

ISSN (online): 2409-5826

Journal of Advanced Thermal Science Research

Decoding Electrocatalysis: Transforming Aluminum-Clad TLC Plates into Potash Alum for Hydrogen Evolution Exploration

Nilankar Diyali, Gopal Sarkar and Bhaskar Biswas*

Department of Chemistry, University of North Bengal, Darjeeling 734013, India

ARTICLE INFO

Article Type: Research Article

Academic Editor: Halil Durak

Keywords:
Activated
Potash alumn
H2 production
Alkaline medium
Heterogeneous electrocatalysis

Timeline:
Received: November 15, 2023
Accepted: December 17, 2023
Published: December 24, 2023

Citation: Diyali N, Sarkar G, Biswas B. Decoding electrocatalysis: Transforming aluminum-clad TLC plates into potash alum for hydrogen evolution exploration. J Adv Therm Sci Res. 2023; 10: 89-97.

DOI: https://doi.org/10.15377/2409-5826.2023.10.7

ABSTRACT

This work deals with using a waste aluminum-based TLC plate to prepare crystalline potash alum, which is subsequently activated for the study of hydrogen evolution reaction in alkaline KOH. The structural and morphological characterization of the synthesized potash alum (PA) has been assessed with powder X-ray diffraction and thermogravimetry analysis. Scanning electron micrographs reveal the morphology of the activated potash alum. The heterogeneous electrocatalytic HER activity in 1 M KOH attributes a moderate electrocatalytic efficiency for activated potash alum (APA) in the light of onset potentials, Faradic efficiency, double-layer capacitance, electrochemically activated surface area, and number of active sites. However, the electrocatalyst APA is a pre-catalyst as it undergoes a significant structural transformation under the electrochemical operation, leading to Al2O3 nanoparticles being the active catalyst for hydrogen production. Possibly, the chemical inertness of the Al2O3 induces a limitation in the local vicinity for the synergistic effect for facile electron transport in alkaline KOH.

*Corresponding Author
Email: bhaskarbiswas@nbu.ac.in
Tel: +(91) 700 337 2248

1. Introduction

In the contemporary world, addressing critical issues like the energy crisis, environmental pollution, and human-induced climate change heavily relies on the intersection of energy and the environment. Scientists globally are searching for clean and renewable energy sources to tackle these pressing concerns [1]. In recent years, significant progress has been made in developing materials with cost-effective properties [2-4], particularly in exploring energy conversion and enhancing storage efficiency on a pilot scale [5, 6]. Electrochemical hydrogen production emerges as a promising solution in response to the urgent need for carbon-free energy, aligning with environmental sustainability goals and economic well-being [7, 8]. Hydrogen, as a clean energy carrier, boasts environmental friendliness, and high energy density and upon combustion, produces water as a byproduct, resulting in zero greenhouse gas emissions [9]. The coordination of compound-driven electrocatalytic hydrogen production has recently garnered significant attention from researchers [9]. Nevertheless, the pursuit of benchmark electrocatalysts remains paramount, emphasizing low overpotential, optimal stability, and durability under electrochemical conditions, cost-effectiveness, and exceptional turnover frequency for the proton reduction reaction, all crucial factors in meeting the growing demand for hydrogen energy [9].

Numerous electrocatalysts involving d-metals have been created for hydrogen generation in acidic and alkaline conditions [9]. Notably, the use of potash alum presents an intriguing avenue. Potassium aluminum sulfate dodecahydrate, known as potash alum (PA), possesses the chemical formula $K_2Al_2(SO_4)_4{\cdot}24H_2O$. As reported previously, the crystal structure of PA typically exhibits a cubic system with the *Pa3* space group. It can adopt different atomic arrangements, classifying into α, β, and γ-type lattices [10-12]. Generally, PA belongs to the α-type with a lattice constant a=12.15 Å [11]. It has been observed that upon heating to 510 K (237 °C), the lattice water molecules in alum can be eliminated, resulting in crystalline $KAl(SO_4)_2$ [13]. Researchers have demonstrated that heating $KAl(SO_4)_2{\cdot}12H_2O$ to 180 °C for two hours induces a transition from a crystalline to an amorphous phase [14]. Additionally, the $KAl(SO_4)_2{\cdot}12H_2O$ powder can be heated to 500 °C for two hours to obtain the anhydrous form, $KAl(SO_4)_2$. The transition from crystalline to amorphous phase in alum starts at approximately 75 °C and is sustained up to around 180 °C, beyond which the anhydrous form may be achieved [15].

PA has a long history of versatile applications in various aspects of daily life, including but not limited to deodorants [16], catalysis [17], food additives [18], and skincare products [19]. It has also been found to be used in optical limiting, switching applications [20], and Raman laser converters [21]. In the study conducted by Hemalatha *et al*., the crystal of potassium aluminum sulfate dodecahydrate was identified to belong to the cubic system with the *Pa3* space group, featuring a lattice constant a=12.24 Å and Z=4 [22]. The crystal exhibited a conductivity of 3.154 × 10−10 S/cm at 308 K. Furthermore, Gu and Li reported that PA crystals could undergo electrolytic colouring below 100 °C at various voltages, utilizing a flat anode and a pointed cathode [23].

In recent research, there has been an exploration of PA for novel medicinal applications. Ali conducted a study investigating the antibacterial properties of alum, as well as the synergistic effects of combining alum with antibiotics to eliminate microbes [24]. Our study focused on the quantitative production of PA from Al-based waste plates. We employed the activated form of PA to examine its electrocatalytic capabilities in hydrogen production in an alkaline KOH environment. Facilitating the generation of H_2 through this method not only accentuates our dedication to environmental consciousness but also illuminates our unwavering commitment to sustainability and the artful stewardship of resources.

2. Materials and Methods

All chemicals and solvents used in the synthesis were of the analytical reagent grade and the highest purity available ~99% pure; potassium hydroxide (Thomas Baker, India), H_2SO_4 Merck), and Aluminium Hydroxide (Merck) were bought from commercial outlets and used without further purification.

The morphology and structural characteristics of the synthetic compounds were determined by powder X-ray diffractometer (Rigaku SmartLab) using Cu-K α radiation with wavelength 1.54 ranging from 10°-80°. The crystalline sample was grounded in the mortar pestle to obtain powders. Then, the sample was placed in the

center of the sample holder and spread to a uniform layer with the help of a glass slide, ensuring the surface was smooth. Finally, the excess powder was removed from the sample holder's edges and carefully placed in the XRD slot.

Thermogravimetric analysis was conducted using TGA Q50 V20.10 Build 36 Module under continuous N_2 flow of 60.0 ml/min. 1.14200 mg of sample was taken in a platinum pan, equilibrated at 30.00 °C, then jumped to 60.00 °C, and kept Isothermal for 10.00 min. Then equilibrated at 30.00 °C followed by ramping at 10.00 °C/min to 800.00 °C.

2.1. Electrochemical Measurements

All the measurements were performed using the RVL PG-Lyte-1.0 electrochemical workstation. A three-electrode setup was used to perform the experiments, including glassy carbon as the working electrode (GCE, 3 mm diameter), platinum wire as the counter electrode, and Ag/Ag^+ as the Reference electrode (saturated with AgCl). The LSVs were run under potential between 0 to -2 V at a scan rate of 5 mV/s. All the potentials represented were against reversible hydrogen electrode (RHE) using the Nernst equation,

$$E_{RHE} = E_{Ag/AgCl} + 0.0591*pH + 0.1976 \quad \text{(S1)}$$

All the data were corrected for iR loss.

2.1.1. Calculation of Active Sites and Turnover Frequency (TOF)

The active sites and turnover frequency (TOF) were calculated for the APA following the equations. Considering the two-electron reduction process from the CV, the absolute components of voltammetric charges (cathodic and anodic) were examined by analyzing the area of the curve of the APA complex. Further, the active sites (n) of the heterogenous catalyst were calculated in mol^{-1}.

$$Charge\ (Q) = \frac{Area\ of\ the\ curve}{2 \times\ Scan\ rate} \quad \text{(S2)}$$

$$n = \frac{Q}{2 \times F} \quad \text{(S3)}$$

The turnover frequency (in s^{-1}) per-sites was calculated using the equation given below:

$$TOF = \frac{I}{F\ n}\frac{1}{2} \quad \text{(S4)}$$

Where I is current (in A) during the LSV, F is Faraday constant (in C mol^{-1}), n is the number of active sites (in mol), and the factor ½ represents a two-electron process in hydrogen production.

2.2. Double-Layer Capacitance

Double layer capacitance for the MOF was determined by measuring the current in the non-faradic region through CV at different rates in the voltage window of 0 V to -0.10 V, followed by plotting a graph between the scan rate and current at the mid-point of the potential window and subsequently linear fitting the curve to obtain the slope i.e. double layer capacitance. This non-faradic region is typically a 0.1 V window about the open circuit potential, and all the measured current values are due to double-layer charging.

The double-layer capacitance (C_{dl}) was calculated using the equation given below:

$$i_c = v\ C_{dl}$$

Where, i_c = Double-layer charging current

v = Scan rate

2.3. Electrochemically Active Surface Area (ECSA)

The AP's electrochemically active surface area (ECSA) was calculated based on the double-layer capacitance mentioned above.

The ECSA was calculated using the equation given below:

$$\text{ECSA} = \frac{C_{dl}}{C_s}$$

Where, C_{dl} = Double-layer capacitance

C_s= specific capacitance of the system (constant factor)

The unit of ECSA is per cm^2.

2.4. Roughness Factor (RF)

The following equation calculates the roughness factor for the APA

$$\text{RF} = \frac{EASA}{Electrode\ geometrial\ area}$$

There is no unit of roughness factor.

3. Results and Discussion

3.1. Synthetic Process of the Potash Alum (PA)

The waste aluminum plates, composed of aluminum, were gathered from the laboratory and thoroughly cleaned by rinsing with deionized water. The resulting waste aluminum was then ground into a powder. Subsequently, 1.15 grams of the aluminum waste were measured and transferred to a beaker containing 250 mL of a 1.4 M KOH solution, followed by gentle heating without boiling. The ongoing reaction generated hydrogen, indicated by visible bubbles. When the reaction concluded, a clear solution with no bubbles was observed. The solution was then cooled in an ice bath and filtered into a 500 mL flask using vacuum filtration.

Next, 250 mL of a 4.0 M H_2SO_4 solution was added to the flask with the filtered solution, and the mixture was slowly heated with stirring to ensure complete dissolution of $Al(OH)_3$. The reaction flask was subsequently allowed to cool in the ice bath for twenty-five minutes. This solution recrystallizes alum, after which the resulting crystals undergo a two-day drying period. Subsequently, the alum crystals are gathered and precisely weighed using an analytical scale, and their mass is recorded.

The overall reactions that take place are as follows:

$$2\ Al(s) + 2\ KOH\ (aq) + 4\ H_2SO_4(aq) + 22\ H_2O(l) \longrightarrow^{\Delta} 2KAl(SO_4)_2.12H_2O(s) + 3H_2(g)$$

3.2. Chemical Test for Qualitative Analysis of Alum

A qualitative examination of the synthesized potash alum is conducted to validate the presence of potassium, sulfate, aluminum, the water of hydration, and the alum melting point. The water of crystallization is present in the artificial alum. In a thermostatically controlled oven, 3.0 g of alum is dried to a consistent weight, and the weight difference is noted.

PA was characterized by various analytical methods, including elemental analysis and powder X-ray diffraction studies (Fig. **1**). The pxrd pattern of the synthesized APA matched the peak in the literature [11, 25].

3.3. Morphological Characteristics and Thermal Analysis of PA

The morphological characterization of the synthetic PA has been principally assessed with PXRD. The PXRD plots for PA (Fig. **1**) displayed distinct peaks within a 2θ value of 40° and presented a prominent crystallinity (JCPDS No. 07-4921).

The APA's thermogravimetric analysis (TGA) was recorded by slowly ramping the temperature from 0 to 400 °C. The incremental mass loss of 45.5 % was observed between 105 °C and 193 °C, accounting for twenty-four water molecules. After 200 °C, the compound was stable, and the mass percentage agreed well with $KAl(SO_4)_2$ (JCPDS No. 74-0082). The results of this study are in excellent agreement with those in the literature [13-15]

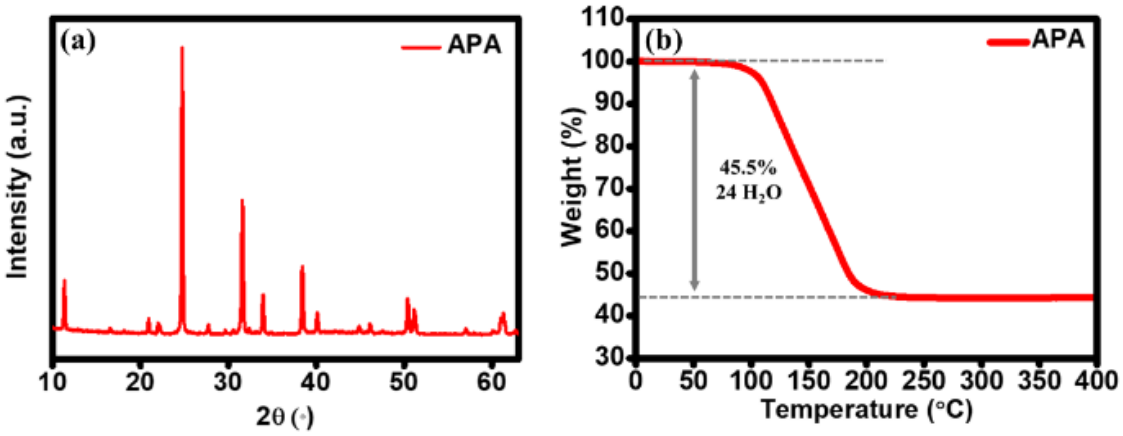

Figure 1: a) PXRD pattern of APA; **b**) TGA plot of APA.

3.4. Electrochemical Studies for Hydrogen Production

The electrochemical properties of the activated potash alum, APA, were studied with a three-electrode setup consisting of modified glassy carbon as the working electrode, platinum (Pt) as a counter electrode, and Ag/AgCl as a reference electrode. The APA was investigated for electrocatalytic hydrogen evolution reaction (HER) in an alkaline condition (1 M KOH solution). The linear sweep voltammetry (LSV) in the cathodic direction was recorded for the complex in 1 M KOH solution with a scan rate (υ) of 5 mV/s. The overpotential(η) value was estimated as 619 mV for APA to reach the current density of 10 mA cm^{-2} (Fig. **2a**).

For a deep understanding of the electrochemical nature of the APA, the Tafel slope was derived from the Tafel plot profiling η against log j by following η = b log j + a, where b and j represent the Tafel slope and current density, respectively (Fig. **2b**). Many researchers in this field expounded on the mechanistic aspects of the alkaline HER through the Tafel slope [9, 20-22, 26]. The Tafel slope value for APA was evaluated at 219 mV dec^{-1}, demonstrating the rate-determining step as the Volmer-Heyrovsky step in electrocatalytic hydrogen evolution (Fig. **2b**). To reveal the kinetic nature of the electrocatalytic hydrogen evolution studies, the onset potential was derived for the APA electrocatalyst, which is 0.209 V.

The estimation of active sites in the electroactive film was pursued with directly related surface area parameters, namely electrochemical double-layer capacitance (C_{dl}), electrochemically activated surface area (ECSA), and roughness factor (R_f) [23, 24]. The C_{dl} of APA electrocatalysts was determined from the CVs at the non-Faradic region recorded at different scan rates (Fig. **2c**). The current values at the middle potential of the non-Faradic area were plotted against the scan rate and the linear slope, which is equivalent to twice the C_{dl} (Fig. **2d**) [27, 28]. The C_{dl} value for APA (0.0708 μF) manifests a higher electrical energy storage capacity for the APA catalyst. Subsequently, electrochemically activated surface area (ECSA) was derived from the equation S2. The ECSA of APA was estimated as 0.00257 $cm^{2,}$ validating the higher electrochemical activity for the complex. Similarly, R_f was determined to be 0.0364 for APA.

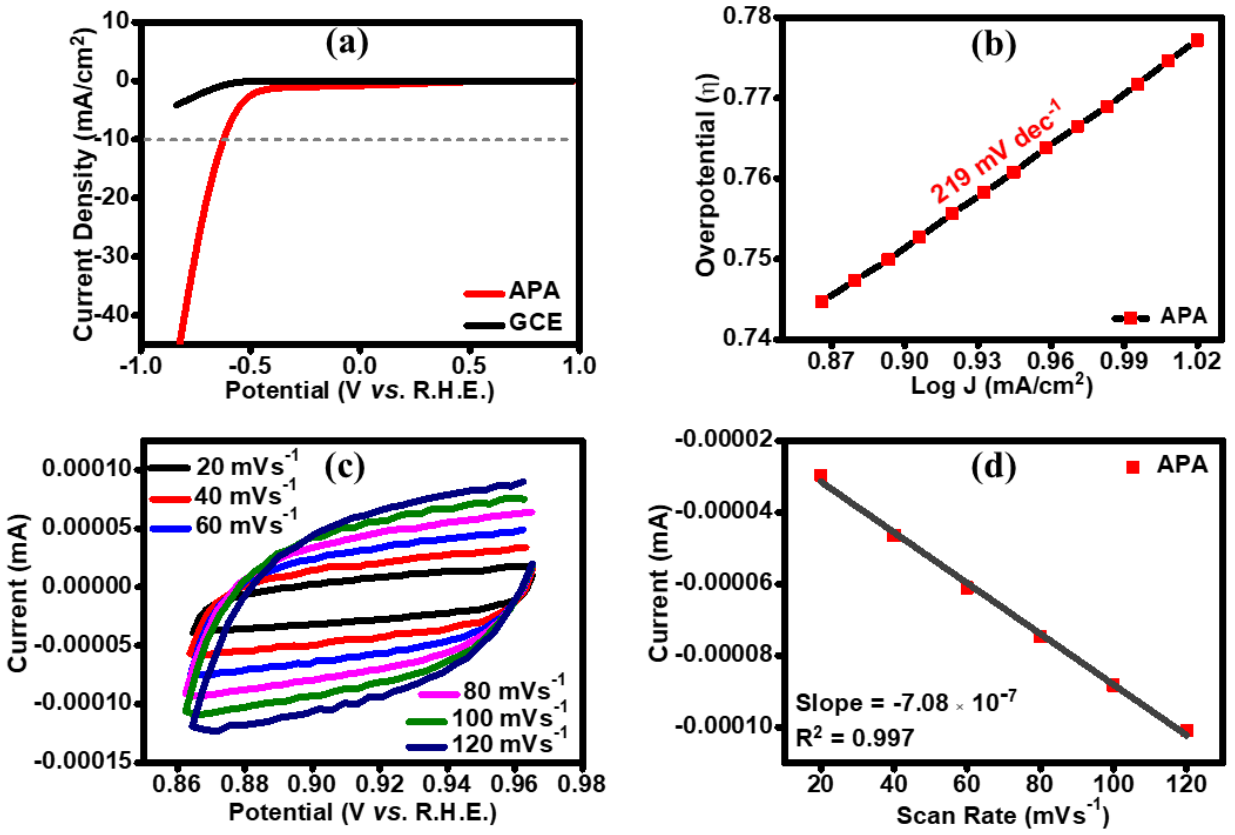

Figure 2: a) LSV of APA (red) and bare glassy carbon electrode (GCE, black); **b**) Tafel plot obtained from the LSV of APA from Fig. (**1a**); **c**) Plot of current *vs.* potential at different scan rates for the determination of double layer capacitance at the non-Faradic region; **d**) Profile of the current vs scan rate variation for the calculation of electrochemical double-layer capacitance.

The intrinsic activity of the APA is administered by calculating the charge (Q), the number of active sites(n), and turnover frequency (TOF) using the equation from the literature [23, 24]. The number of active sites (n) for APA was evaluated as 3.97×10^{-8} mol, respectively, while TOFs were calculated as 0.06525 s^{-1}. The electrochemical parameters viz overpotential (η), Tafel slope (b), TOF, $C_{dl,}$ ECSA, and R_f of APA electrocatalyst are tabulated in (Table **1**).

Table 1: HER Parameter.

Catalyst	Overpotential (η) @ 10mA/cm²	Tafel Slope (mV/dec)	TOF (s^{-1})	Onset (V)	C_{dl} (μF)	ECSA (cm^2)	R_f
APA	619	219	0.06525	209	0.0708	0.00257	0.0364

The electrochemical stability and durability of the synthetic APA catalysts for hydrogen production in alkaline water splitting have been executed with chronoamperometry. The chronoamperometry was allowed to run for 3 h at a 10 mA/cm^2 current density for APA in 1 M KOH. The chronoamperometry plots are displayed in (Fig. **3a**). The chronoamperometry plot for APA showed a slow fall in the current density over 3 hours, which may have accounted for the peeling off of the catalyst from the catalyst surface due to bubble accumulation and release. To understand the role of the active species, the pxrd of the recovered catalyst was taken. The pxrd pattern of the recovered catalyst displayed new peaks, suggesting the transformation of the APA to the active catalyst during the HER (Fig. **3b**).

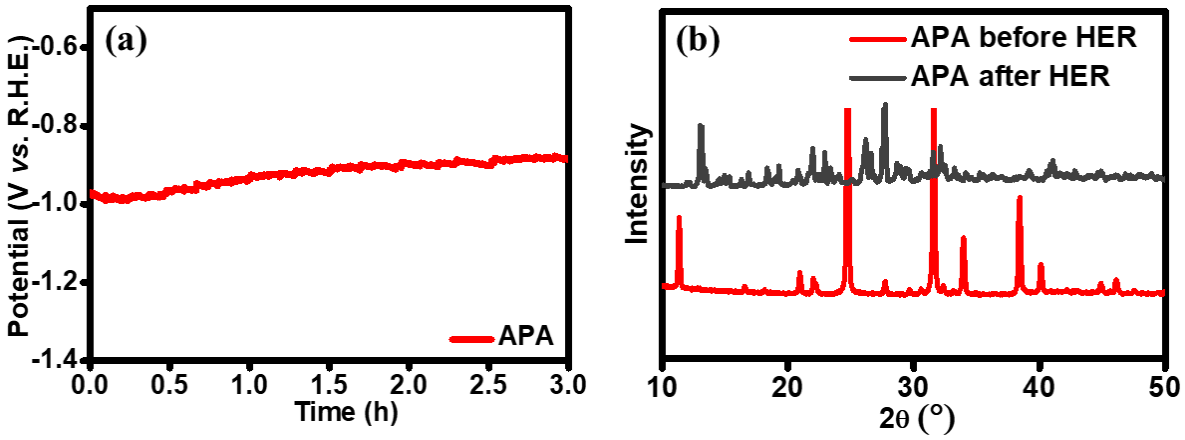

Figure 3: a) Chronoamperometry plot of APA at the current density of 10 mA/cm^2; **b**) PXRD pattern of the APA before HER and APA after HER.

4. Conclusion

In conclusion, our careful use of discarded aluminum has created APA, an effective catalyst. This catalyst demonstrates an outstanding capability to accelerate the hydrogen evolution reaction, overseeing the production of H_2 in a way that not only prioritizes environmental awareness but also underscores dedication to sustainability and inventive resource management. The APA catalyst marks an overwhelming performance in electrochemical alkaline HER in 1 M KOH in the light of excellent current density, low onset potential (0.209 V), large electrochemical double-layer capacitance (0.0708 μF), higher electrochemical activated surface area (0.00257 cm^2) and high TOF, 0.06525 s^{-1}. The estimated Tafel slope, 209 mV dec^{-1} for the APA-electrocatalyst, features the Volmer-Heyrovsky kinetics for hydrogen evolution. The chronoamperometry analysis for 3h suggests a dramatic structural transformation under the electrochemical condition and points out the pre-catalytic nature of the complex. The PXRD pattern of the recovered electrocatalyst displayed the signature peaks of the aluminum oxide and consolidated the development of an active catalyst. We anticipate that the APA electrocatalyst would be the first report/limited edition for potash alum-based electrocatalysts in alkaline HER under the gravity of superior working efficiency and long-term electrochemical stability.

Author Contributions

N. Diyali: Conceptualization, Formal analysis, Methodology, Investigation; G. Sarkar: Formal analysis, Investigation; B. Biswas: Conceptualization, Writing-Reviewing and Editing, Supervision.

Conflicts of Interest

There are no conflicts to declare.

Funding

BB acknowledges the Science and Engineering Research Board (SERB), India, for financial support under the EMEQ scheme (EEQ/2020/000079).

Acknowledgments

ND thanks UGC, India, for providing the fellowship (231610208373).

References

[1] Arsalis A, Alexandrou A. Effect of collector tilt angle on the performance of a residential solar-heating-and-cooling system. J Adv Therm Sci Res. 2015; 1: 44-50. https://doi.org/10.15377/2409-5826.2014.01.02.2

[2] Gingu O, Harabor A, Rotaru P, Pascu I, Ciupitu I, Benga G, *et al*. Influence of two steps sintering parameters on tribological behavior of hybrid hydroxyapatite-based biocomposites. J Adv Therm Sci Res. 2015; 1: 66-70. https://doi.org/10.15377/2409-5826.2014.01.02.5

[3] Rasaily S, Sharma D, Pradhan S, Diyali N, Chettri S, Gurung B, *et al*. Multifunctional catalysis by a one-dimensional copper(II) metal-organic framework containing pre-existing coordinatively unsaturated sites: Intermolecular C–N, C–O, and C–S Cross-Coupling; Stereoselective intramolecular C–N coupling; and aziridination reactions. Inorg Chem. 2022; 61: 13685-99. https://doi.org/10.1021/acs.inorgchem.2c00270

[4] Diyali N, Rasaily S, Biswas B. Metal–organic framework: An emergent catalyst in C–N cross-coupling reactions. Coord Chem Rev. 2022; 469: 214667. https://doi.org/10.1016/j.ccr.2022.214667

[5] Jiang F, Zeng J, Wu W, Peng P. Direct numerical simulation modeling of multidisciplinary transport during li-ion battery charge/discharge processes. J Adv Therm Sci Res. 2014; 1(2): 32–43. https://doi.org/10.15377/2409-5826.2014.01.02.1

[6] Elishav O, Mosevitzky Lis B, Miller EM, Arent DJ, Valera-Medina A, Grinberg Dana A, *et al*. Progress and prospective of nitrogen-based alternative fuels. Chem Rev. 2020; 120: 5352-436. https://doi.org/10.1021/acs.chemrev.9b00538

[7] Dawood F, Anda M, Shafiullah GM. Hydrogen production for energy: An overview. Int J Hydrogen Energy. 2020; 45: 3847-69. https://doi.org/10.1016/j.ijhydene.2019.12.059

[8] Wang J, Xu F, Jin H, Chen Y, Wang Y. Non-noble metal-based carbon composites in hydrogen evolution reaction: Fundamentals to applications. Adv Mater. 2017; 29(14): 1605838. https://doi.org/10.1002/adma.201605838

[9] Diyali S, Diyali N, Biswas B. Coordination-driven electrocatalysts as an evolving wave of enthusiasm for sustainable hydrogen production. Coord Chem Rev. 2024; 500: 215496. https://doi.org/10.1016/j.ccr.2023.215496

[10] Wijayati N, Lestari LR, Wulandari LA, Mahatmanti FW, Rakainsa SK, Cahyono E, *et al*. Potassium Alum [$KAl(SO_4)_2{\cdot}12H_2O$] a solid catalyst for effective and selective methoxylation production of alpha-pinene ether products. Heliyon. 2021; 7: E06058. https://doi.org/10.1016/j.heliyon.2021.e06058

[11] Abdulwahab AM, Al-magdashi YAA, Meftah A, Al-Eryani DA, Qaid AA. Growth, structure, thermal, electrical, and optical properties of potassium aluminum sulfate dodecahydrate (potash alum) single crystal. Chinese J Phys. 2019; 60: 510-21. https://doi.org/10.1016/j.cjph.2019.05.034

[12] Souza R, Navarro R, Grillo AV, Brocchi E. Potassium alum thermal decomposition study under non-reductive and reductive conditions. J Mater Res Technol. 2019; 8: 745-51. https://doi.org/10.1016/j.jmrt.2018.05.017

[13] Wojciechowska R, Wojciechowski W, Kamiński J. Thermal decompositions of ammonium and potassium alums. J Therm Anal. 1988; 33: 503-9. https://doi.org/10.1007/BF01913929

[14] Kishimura H, Imasu Y, Matsumoto H. Dehydration of potassium alum induced by shock loading. J Phys Conf Ser. 2014; 500: 182020. https://doi.org/10.1088/1742-6596/500/18/182020

[15] Kishimura H, Imasu Y, Matsumoto H. Thermal dehydration of potash alum studied by Raman spectroscopy and X-ray diffraction analysis. Mater Chem Phys. 2015; 149: 99-104. https://doi.org/10.1016/j.matchemphys.2014.09.049

[16] Alzomor AK, Moharram AS, Al Absi NM. Formulation and evaluation of potash alum as deodorant lotion and after shaving astringent as cream and gel. Int Curr Pharm J. 2014; 3: 228-33. https://doi.org/10.3329/icpj.v3i2.17512

[17] Dubasi N, Varala R, Bollikolla H, Kotra V. Applications of Alum ($KAl(SO_4)_2.12H_2O$) in organic synthesis and as catalysis: A quinquennial update. J Chem Rev. 2023; 5: 263-80.

[18] Yokel R. Aluminum in Food – The nature and contribution of food additives. In: El-Samragy Y, Ed., Food Additive. USA: University of Kentucky; 2012, PP. 205-28. http://dx.doi.org/10.5772/30847

[19] Paigude T. Formulation and evaluation of alum toner spray for anti-acne effect. Int J Creat Res Thoughts. 2023; 11: 456–68.

[20] Farmani AA, Nasirpouri F. Boosting hydrogen and oxygen evolution reactions on electrodeposited nickel electrodes: Via simultaneous mesoporosity, magnetohydrodynamics and high gradient magnetic force. J Mater Chem A. 2020; 8: 24782-99. https://doi.org/10.1039/D0TA06906J

[21] Debnath A, Diyali S, Das M, Panda SJ, Mondal D, Dhak D, *et al*. Harnessing the hydrogen evolution reaction (HER) through the electrical mobility of an embossed Ag(i)-molecular cage and a Cu(ii)-coordination polymer. Dalton Trans. 2023; 52: 8850-6. https://doi.org/10.1039/D3DT01073B

[22] Diyali S, Diyali N, Das M, Joshi M, Ray PP, Sher Shah MdSA, *et al*. Supramolecular Framework-Driven Electrical Conductivities and Hydrogen Evolution Activities of Hybrid Nickel(II)–Cerium(IV) Complex Salts Cooperativity. Cryst Growth Des. 2022; 22: 7590-602. https://doi.org/10.1021/acs.cgd.2c01115

[23] Raveendran A, Chandran M, Dhanusuraman R. A comprehensive review on the electrochemical parameters and recent material development of electrochemical water splitting electrocatalysts. RSC Adv. 2023; 13: 3843-76. https://doi.org/10.1039/D2RA07642J

[24] Yu F, Yu L, Mishra IK, Yu Y, Ren ZF, Zhou HQ. Recent developments in earth-abundant and non-noble electrocatalysts for water electrolysis. Mater Today Phys. 2018; 7: 121-38. https://doi.org/10.1016/j.mtphys.2018.11.007

[25] Werner P-E, Erikson L, Westdahl M. Program TREOR-5, Institute of Inorganic Chemistry, University of Stockholm, Sweden, 1988.

[26] Shinagawa T, Garcia-Esparza AT, Takanabe K. Insight on Tafel slopes from a microkinetic analysis of aqueous electrocatalysis for energy conversion. Sci Rep. 2015; 5: Article number: 13801. https://doi.org/10.1038/srep13801

[27] Mohanty B, Ghorbani-Asl M, Kretschmer S, Ghosh A, Guha P, Panda SK, *et al*. MoS2 quantum dots as efficient catalyst materials for the oxygen evolution reaction. ACS Catal. 2018; 8: 1683-9. https://doi.org/10.1021/acscatal.7b03180

[28] Zhou Z, Wei L, Wang Y, Karahan HE, Chen Z, Lei Y, *et al*. Hydrogen evolution reaction activity of nickel phosphide is highly sensitive to electrolyte pH. J Mater Chem A. 2017; 5: 20390-7. https://doi.org/10.1039/C7TA06000A